Research Article

Experiment Analysis of Concrete's Mechanical Property Deterioration Suffered Sulfate Attack and Drying-Wetting Cycles

Wei Tian and Nv Han

School of Civil Engineering, Chang'an University, Xi'an 710061, China

Correspondence should be addressed to Wei Tian; tianwei_816@163.com

The mechanism of concrete deterioration in sodium sulfate solution is investigated. The macroperformance was characterized via its apparent properties, mass loss, and compressive strength. Changes in ions in the solution at different sulfate attack periods were tested by inductively coupled plasma (ICP). The damage evolution law, as well as analysis of the concrete's meso- and microstructure, was revealed by scanning electron microscope (SEM) and computed tomography (CT) scanning equipment. The results show that the characteristics of concrete differed at each sulfate attack period; the drying-wetting cycles generally accelerated the deterioration process of concrete. In the early sulfate attack period, the pore structure of the concrete was filled with sulfate attack products (e.g., ettringite and gypsum), and its mass and strength increased. The pore size and porosity decreased while the CT number increased. As deterioration progressed, the swelling/expansion force of products and the salt crystallization pressure of sulfate crystals acted on the inner wall of the concrete to accumulate damage and accelerate deterioration. The mass and strength of concrete sharply decreased. The number and volume of pores increased, and the pore grew more quickly resulting in initiation and expansion of microcracks while the CT number decreased.

1. Introduction

Concrete is an important construction material that has been extensively researched and developed over many decades. The durability of concrete structures depends on environmental conditions. Sulfate attacks are a primary chemical attack of concrete, and thus analyzing their impact can help to elucidate the durability of concrete structures and predict their service life as they are subject to damage and deterioration. The main hydration products of cement and sulfate react to generate expansive products resulting in loss of strength [1–4]. The drying-wetting cycle can accelerate this process. The causes and mechanisms of sulfate attack deterioration have been researched extensively from the perspective of sulfate attack alone [5–12] as well as the coupling of drying-wetting cycles and sulfate attack [13–15].

Concrete is deteriorated under sulfate attack because the sulfate ions pass through the pores and the material components undergo a chemical reaction. This leads to the initiation and expansion of pores/cracks and loss of strength [16]. The macromechanics at work during the damage process can be determined by measuring the internal pore structure changes under different deterioration conditions. Many researchers have used the mercury intrusion porosimetry (MIP), nitrogen adsorption, scanning electron microscopy (SEM), and other methods to study this process; the distribution of pores' measurements is relatively accurate over a wide range of measurements. However, traditional microresearch methods have notable drawbacks. The specimen preparation process typically results in grinding damage because the initial state distribution of pores in the same concrete specimen cannot be repeated. X-ray CT scanning technology is an effective and nondestructive technique for observing material microstructures. Yuan et al. [15] studied sulfate attack and drying-wetting cycles to observe the concrete's mesodamage process using CT. Qian et al. [17] used nanoindentation and micro-CT to research concrete pore and mechanical properties under sulfate attack. Naik et al. [18] studied the effects of cement type and water-to-cement ratio on concrete sulfate attack by micro-CT and XRD. El-Hachem et al. [19] identified sulfate

attack products and cracks at different points in the attack process via X-ray microtomography.

Despite these and other valuable contributions to the literature, however, these current studies are generally limited to two-dimensional pore structure evolution characteristics under the sulfate attack environment. Accordingly, further research is necessary concerning the three-dimensional pore structure evolutions, as well as the relationship between the mechanical properties of concrete material and its microstructure. In this paper, we investigated deterioration in concrete specimens subjected to sulfate attack per the macroscopic physical mechanical properties of the material. The mesostructure of the concrete was characterized using the CT technique, and then the three-dimensional (3D) pore structure of the concrete was reconstructed with digital image processing (DIP) technology. The variation in porosity and pore distribution characteristics was quantitatively analyzed, and then pore regional division methods were established accordingly. The relationship between the damage mechanical properties of concrete material and its microstructure was analyzed under the coupling of sulfate attack and drying-wetting cycles.

2. Experimental Procedure

2.1. Experiment Materials and Specimen Preparation. The materials used to be of the Chinese medium-heat Ordinary Portland cement 42.5R produced by Shanxi Jidong Cement Limited Company were adopted. The coarse aggregate was Shanxi Province Yang gao crushed stone with a diameter within 5–30 mm; the fine aggregate was Shanxi Province Yang gao natural river sand with a diameter of 0–5 mm. A naphthalene-based superplasticizer was applied to produce fresh concrete with improving workability. The mix proportions by weight of concrete specimens were listed in Table 1. We made cubic specimens for compressive strength and for mass loss tests. Figure 1 shows the main concrete specimens. Cubic plain concrete specimens ($100 \times 100 \times 100$ mm) were cast in steel molds. After 24 h, all the specimens were demolded and cured at 25°C and 95% relative humidity for 28 days in a standard curing room.

2.2. Experiment Methods. In order to obtain the experimental results more quickly, the specimens were kept in Na_2SO_4 mixed solution with 15% concentration (by mass) and pH 3. Since the pH values of the solutions were changing with the conditioning continued, acids were measured with a pH meter every 8 hours to ensure a pH value constant, and acidity was recorded by DZS-708 Acidometer (Figure 2).

The concrete specimens were immersed in the solution for 60 hours and then placed in a drying oven for 10 hours at 60°C followed by another 4-hour cooling process (Figure 3). The specimens were then soaked in sulfate solution for 16 hours. This process was repeated over 3 days to complete one drying-wetting cycle. Drying-wetting cycles were continued for 63 days. The dimensions of specimens for the test of compressive strength, mass loss, and CT were $100 \times 100 \times 100$ mm. It was important to note that all experiments are performed on three specimen replicates.

Table 1: Mix proportion of concrete specimens.

Materials	Cement	Aggregate	Sand	Water	Superplasticizer
Content (kg/m^3)	311.11	1091.38	857.51	140	2.1

Figure 1: Concrete specimens exposed to drying-wetting cycles with sulfate attack.

Figure 2: DZS-708 Acidometer.

2.2.1. Visual Appearance. The visual appearance of the concrete specimens immersed in sodium sulfate solution was periodically examined to check for spalling, cracking, expansion, and mass loss due to sulfate attack.

2.2.2. Mass Loss Test. According to the GB/T50082-2009 [20] method, mass of the specimens at each sulfate attack period was measured on an electronic scale with an accuracy of 0.01 g.

2.2.3. Uniaxial Compressive Strength Test. We also measured the average compressive strength of three specimens per batch subjected to sulfate solutions according to the GB/T50081-2002 [21] method. The compressive test was carried out on an electrohydraulic servo compressive testing system (WAW3100, Figure 4) with a capacity of 1000 kN. An
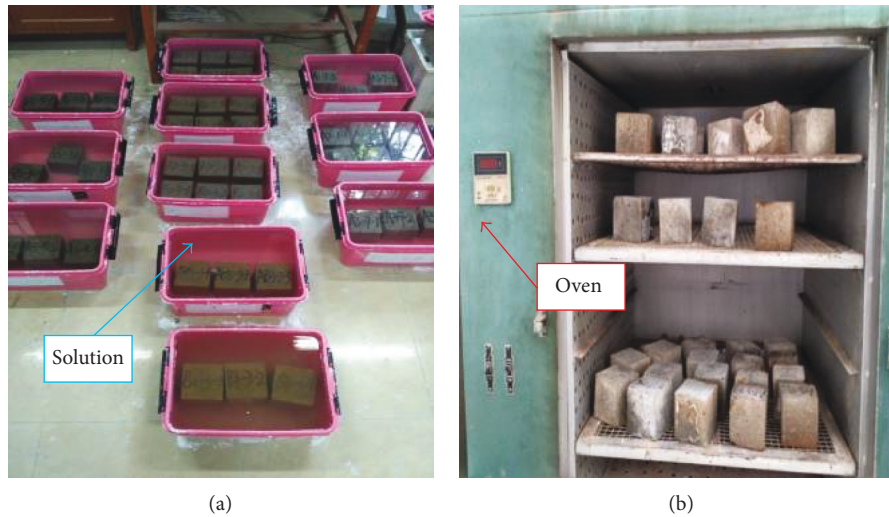
(a) (b)

FIGURE 3: Drying-wetting cycle process.

FIGURE 4: WAW3100 electrohydraulic servo testing system.

antifriction measure was taken by using a PTFE plastic board and carbon dust between loading plates. Tests were conducted in the stress-controlled mode at a loading rate of 0.5 MPa/s until failure.

2.2.4. X-Ray CT Test. The X-ray CT device used in this test was a Toshiba Aquilion One computed tomography scanner at Shaanxi Province Hospital (Figure 5). The internal structures of the concrete specimens (with the dimensions of $100 \times 100 \times 100$ mm) were tested at 0, 21, 42, and 63 days of sulfate attack. The specimens were scanned at 0.5 mm interval, and representative four scanning cross sections of the specimen were selected to analyze in this study (Figure 6). The dimensions of the gray images were 1024×1024 pixel^2, and the minimum resolution was 0.1 mm.

2.2.5. SEM and XRD Test. Scanning electron microscopy (SEM) and X-ray diffraction (XRD-Empyrean) were used to investigate and analyze the microstructure of the specimens

that underwent sulfates attack. The specimens used for SEM observations were 2 cm thick slices from the concrete prisms. The pressure in the specimen chamber was 50 Pa, and the accelerating voltage was 20 kV. After grinding into powder, the cement paste was investigated by XRD to analyze the change in reaction products after sulfate attack.

3. Results and Analysis

3.1. Visual Appearance. Figure 7 shows images of the surface damage characteristics of specimens exposed to sodium sulfate solutions for 63 days. After 21 days of sulfate attack, the concrete surface showed white sodium sulfate crystals so that the surface of the concrete precipitation was "frosted." This is because the saturated sodium sulfate solution directly crystallized, and the chemical reaction products were hydrated to produce crystal products accompanied by physical deterioration. The specimen surfaces were generally coarse at this point. After 42 days of sulfate attack, honeycomb pores were generated, and the edges and corners of specimens showed sanding phenomena and pitting deterioration. After 54 days of sulfate attack, the pitting deterioration depth markedly increased, and several microcracks appeared on the specimen surface from the edges and corners. The cement was dissolved, and coarse aggregates were seen at the edges. After 63 days of sulfate attack, the specimens became severe loose and powdery.

The surfaces of the concrete specimens underwent sulfate attack, and drying-wetting cycle treatments were observed under a Zeiss Stemi 508 3D high-depth stereo microscope (Figure 8). This was enlarged 60-fold for analysis as shown in Figure 9. As expected, more crystals appeared on the specimen pores as the drying-wetting cycles progressed. At 42 days of sulfate attack, expansive products in the solution filled the pores of the material with a white precipitate. The cracks initiated and propagated from the pores. At 54 days of sulfate attack, the surface became rough, and the edges of the pores became blurred. After 63 days of sulfate attack, the aggregate was ejected from the surface, and cracks rapidly propagated from the pores.
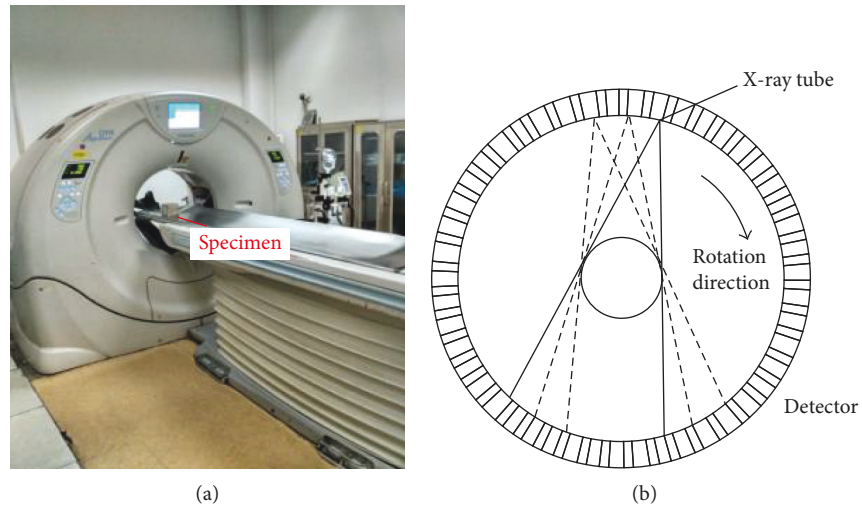
(a)

(b)

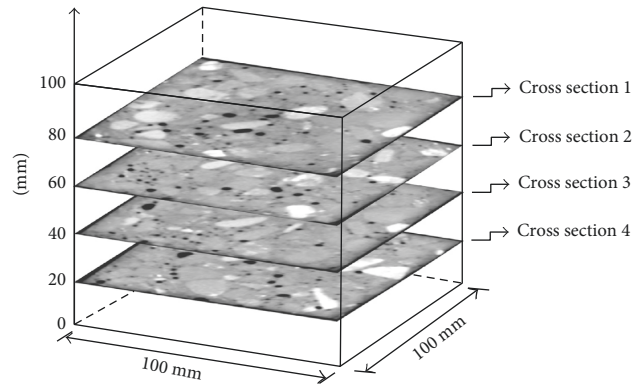Figure 5: A schematic diagram of CT scanner process and the sketch of its working principle.

Figure 6: Location of scanning cross section.

(a)   (b)   (c)   (d)   (e)
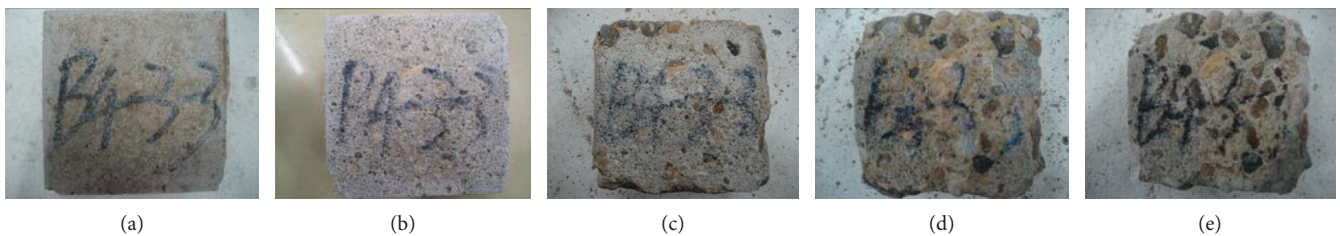
Figure 7: Surface damage characteristics of specimens exposed to drying-wetting cycles with sulfate attack. (a) 0 days, (b) 21 days, (c) 42 days, (d) 54 days, and (e) 63 days.

3.2. Mass and Uniaxial Compressive. Figure 10 shows the variations in mass and compressive strength in concrete exposed to drying-wetting cycles with sulfate attack. It was shown that the variation in mass experienced two periods. In the early period of sulfate attack, the mass of the concrete specimens increased. This was because the solution reacted with the cement hydration products, filled the material's pores, and increased its mass. In the late period of sulfate attack, the mass continued to decrease as hydration products

such as C-S-H and calcium hydroxide gradually dissolved from the surface and specimens became severe loose and sanding.

The uniaxial compressive strength of the specimens' presented "up-down" trend as the sulfate attack period progressed. Initially, the hydration expansive products ettringite, gypsum, and sulfate crystals filled the pores to improve the specimen's density and strength. Then, the expansion force of ettringite and gypsum and the

FIGURE 8: Stemi 508 stereo microscope.

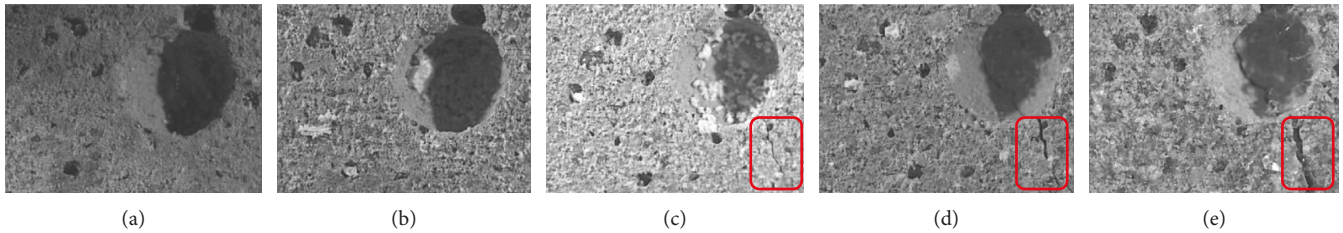(a)   (b)   (c)   (d)   (e)

FIGURE 9: The microscope photographs of surface damage in concrete exposed to drying-wetting cycles with sulfate attack. (a) 0 days, (b) 21 days, (c) 42 days, (d) 54 days, and (e) 63 days.
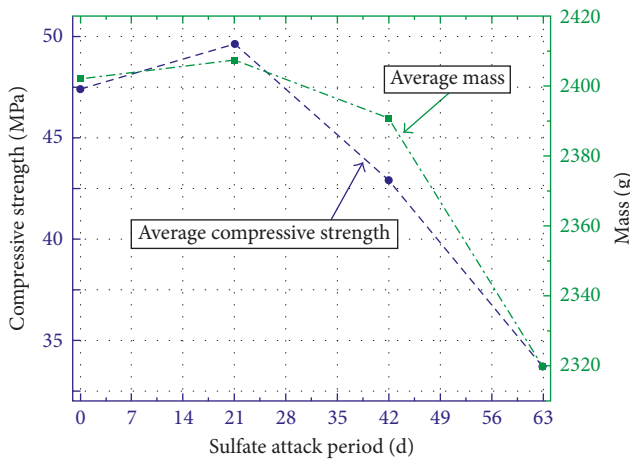

FIGURE 10: The variation of mass and compressive strength in concrete exposed to drying-wetting cycles with sulfate attack.

FIGURE 11: Variation of Ca^{2+} and Mg^{2+} ion value in concrete exposed to drying-wetting cycles with sulfate attack.

crystallization pressure produced by sulfate crystallization then began to act on the pore walls. When the pressure of the pore wall exceeded the concrete's tensile strength, many internal microcracks appeared and decreased the uniaxia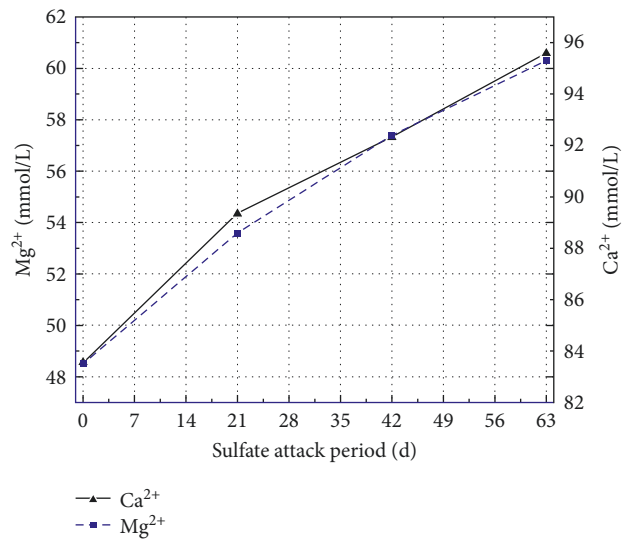l compressive strength. The deterioration of macroscopic mechanical properties was attributed to the combined action of specimens in the acidic sulfate solution and drying-wetting cycles.

(a)   (b)   (c)

(d)   (e)
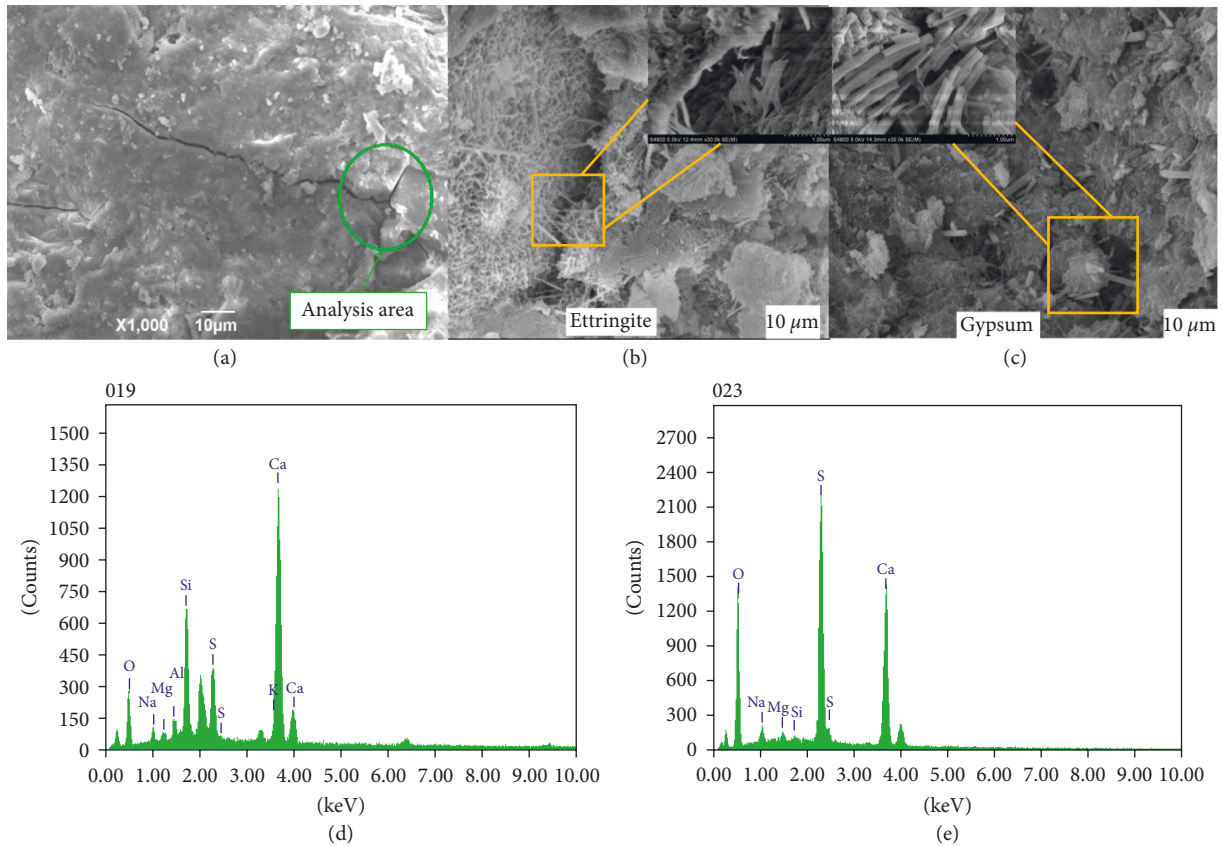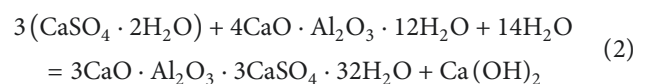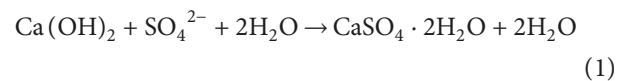
FIGURE 12: (a) SEM of thin sections from DW-1 specimen before chemical exposure, (b) SEM image from DW-1 specimen with ettringite, (c) SEM image from DW-1 specimen with gypsum in cracks and pores, (d) EDX analysis of squared area in (b) showing ettringite components, and (e) EDX analysis of squared area in (c) showing gypsum components.

3.3. Ion Concentration. The concentrations of Ca^{2+} and Mg^{2+} in the solution dissolved due to a series of water chemistry reactions after 63 days of sulfate attack (Figure 11). These ions' concentrations were high at the initial period of sulfate attack, and then the calcium hydroxide and magnesium hydroxide on the surface of the concrete specimen rapidly dissolved in the acid solution. The dissolution rate of calcium and magnesium ions decreased slightly as the pores grew in size and number with better-connected infiltration pathways.

3.4. SEM Result Analyses. Figures 12 and 13 shows SEM images of the concrete subjected to a sodium sulfate solution for 63 days. The needle-shaped ettringite and short columnar gypsum crystals of the sulfate attack products were found in the cracks and inner pores of the specimen. The formation of these products not only reduced the bond strength between the aggregates and mortar but also continually caused swelling, cracking, and spalling. The EDS spectra indicated that the expansive products were aluminum, sulfur, calcium, silicon, and other elements. The main elements were trace elements of gypsum and ettringite. The XRD patterns of the specimens show typical crystals and phases of hydrated cement. After sulfate attack, large amounts of expansive products such as gypsum and ettringite were produced, while the main hydration

products such as C-S-H and $Ca(OH)_2$ gradually dissolved or decomposed—this destroyed the bonds between the aggregates and mortar and damaged the specimens. This reveals the presence of gypsum ($CaSO_4 \cdot 2H_2O$) and ettringite ($3CaO \cdot Al_2O_3 \cdot 3CaSO_4 \cdot 32H_2O$) that formed via the following equations:

$$Ca(OH)_2 + SO_4^{2-} + 2H_2O \rightarrow CaSO_4 \cdot 2H_2O + 2H_2O \tag{1}$$

$$3(CaSO_4 \cdot 2H_2O) + 4CaO \cdot Al_2O_3 \cdot 12H_2O + 14H_2O$$
$$= 3CaO \cdot Al_2O_3 \cdot 3CaSO_4 \cdot 32H_2O + Ca(OH)_2 \tag{2}$$

3.5. CT Test Result Analyses. CT was used to characterize the changes in the internal structure of the concrete specimens at different sulfate attack periods. CT data were analyzed with the visualization software ENVI®. Through this strategy, the pore and crack distributions of different specimen cross sections as a function of sulfate attack period may be determined. Numerous 2D images were obtained from each specimen. Thus, we chose representative specimens labeled DW-1 and DW-2 images to analyze (Figure 14). It was noted that these image processing methods were not described in this study, and more research content can be found in our previous study [22].
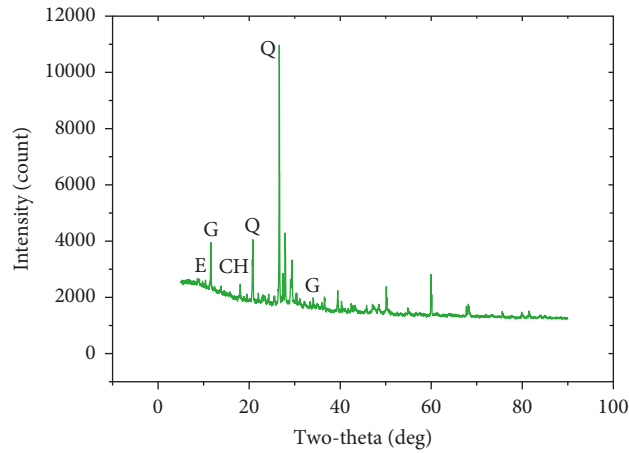
FIGURE 13: XRD of powder specimen from DW-1 specimen after 63 days sulfate attack. (E = ettringite, CH = calcium hydroxide, G = gypsum, Q = quartz).
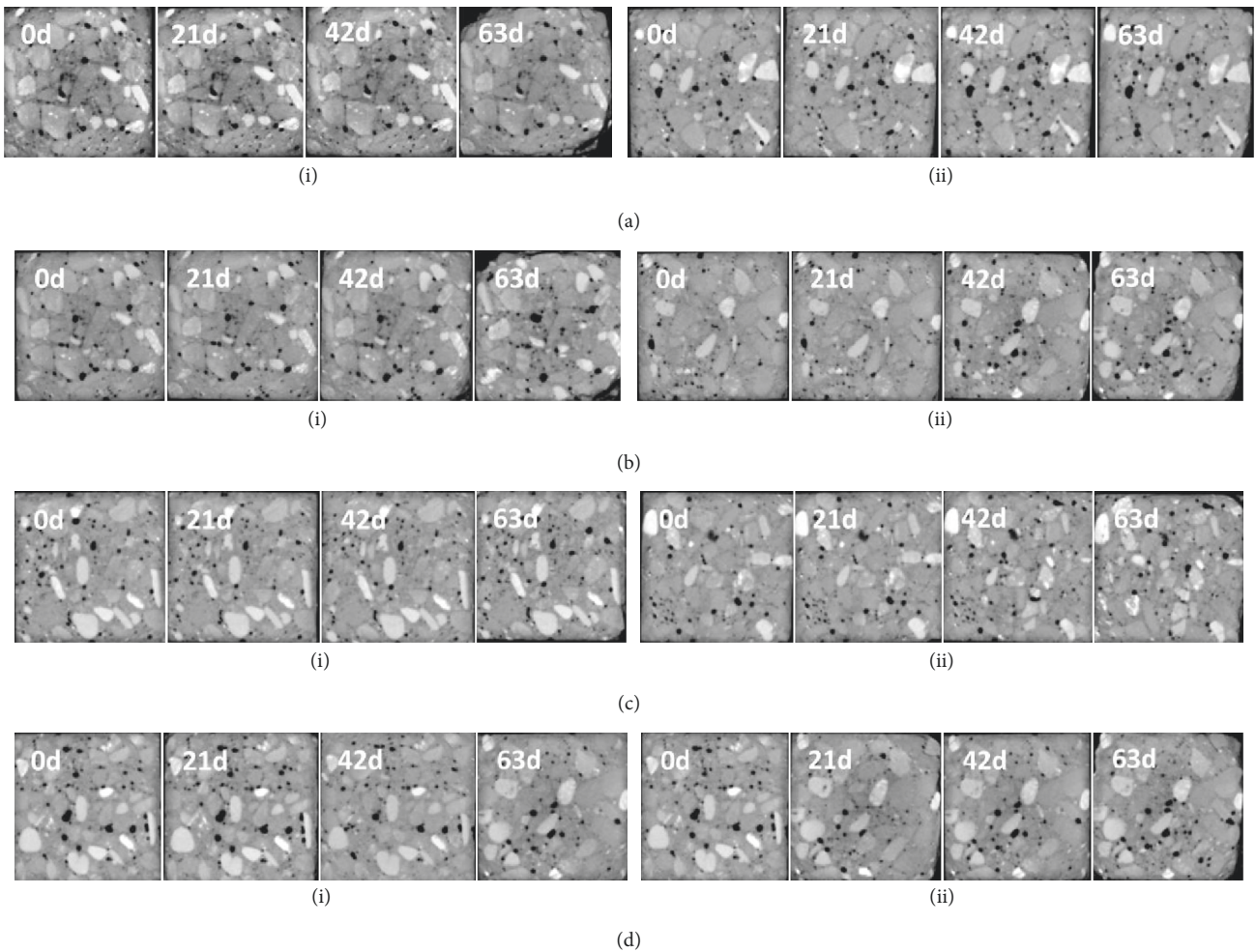

FIGURE 14: Cross-section CT images of DW-1 and DW-2 exposed to drying-wetting cycles with sulfate attack. (a) (i) Cross-section CT images of DW1-1 under different sulfate attack periods; (ii) cross-section CT images of DW2-1 under different sulfate attack periods. (b) (i) Cross-section CT images of DW1-2 under different sulfate attack periods; (ii) cross-section CT images of DW2-2 under different sulfate attack periods. (c) (i) Cross-section CT images of DW1-3 under different sulfate attack periods; (ii) cross-section CT images of DW2-3 under different sulfate attack periods. (d) (i) cross-section CT images of DW1-4 under different sulfate attack periods; (ii) cross-section CT images of DW2-4 under different sulfate attack periods.
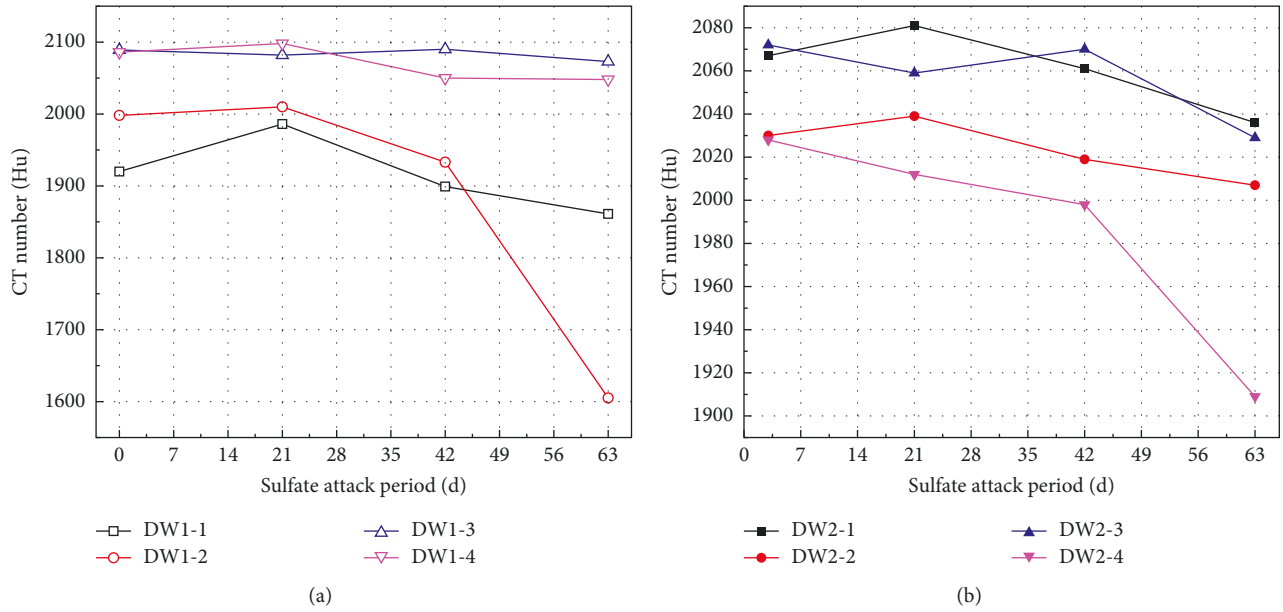
FIGURE 15: Variation of the average CT numbers of DW-1 and DW-2 exposed to drying-wetting cycles with sulfate attack.
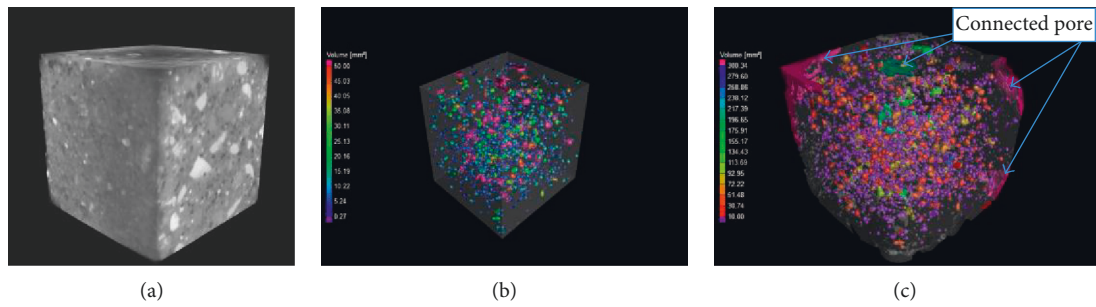

FIGURE 16: 3D reconstructed concrete and pores. (a) 3D concrete (aggregates in white and pores in black). (b) 3D pore without sulfate attack. (c) 3D pore at the 63-day sulfate attack.

TABLE 2: Statistical results of pore characteristics of DW-1 exposed to drying-wetting cycles with sulfate attack.

Specimen	D-W cycle	Volume porosity (%)	Pore number
	0	1.89	846
DW-1	21	1.67	896
	42	2.06	797
	63	2.16	917

TABLE 3: Statistical results of pore characteristics of DW-2 exposed to drying-wetting cycles with sulfate attack.

Specimen	D-W cycle	Volume porosity (%)	Pore number
	0	2.21	956
DW-2	21	2.07	855
	42	3.41	753
	63	3.67	987

3.5.1. CT Number Analysis Results. CT number (CTN) in Hounsfield units represents the mean X-ray absorption which is related to the density of materials. The average CTN of the concrete samples' cross sections ranged from −1600 to 2100. The relationship curve between average CTN and sulfate attack period of DW-1 and DW-2 is shown in Figure 15. The average CTN increased throughout the early period (to day 21) of sulfate attack. Ettringite, gypsum, and sulfate crystals filled the specimen's micropores and increased the overall density. There were no significant changes in the CT images at 42 days of sulfate attack, but the CTNs did decrease as the swelling force of the sulfate attack

products acted on the pore walls, and the pores size were slightly expanded. There was accumulating damage that accelerated the deterioration rate in the specimens. At 63 days of sulfate attack, the CTN decreased significantly. The values of the sections decreased by 19.6% and 5.86% for DW-1 and DW-2, respectively. The reason may be denser edges, and corners of the specimens were sanded by sulfate attack, which caused the CTN decreased.

3.5.2. Pore Characteristic Analysis Results. The 3D pore structures were reconstructed by *VGStudio MAX 2.0*
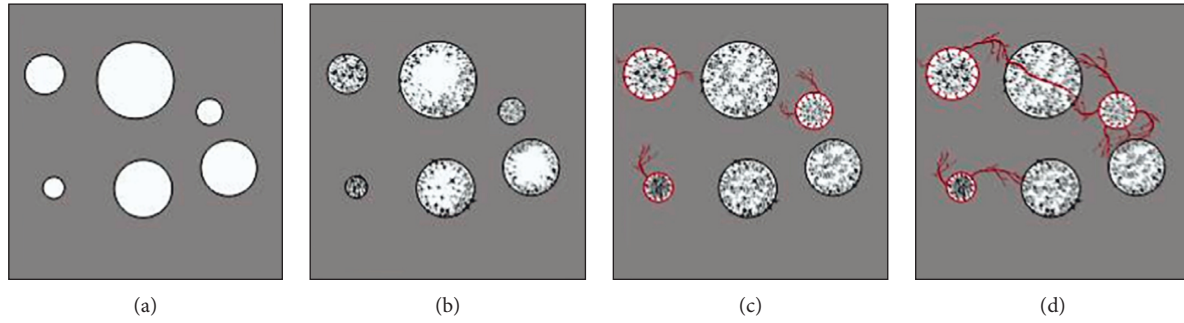
FIGURE 17: The pore evolution rules of concrete specimens exposed to drying-wetting cycles with sulfate attack. (a) Initial stage, (b) filling stage, (c) expanded stage, and (d) connected stage.

software. The surface fit function was used to set the proper thresholds (the pore threshold was set as −831 to −1292 HU) and segment the images into two phases at which point we could calculate porosity using the volume analysis tool. The information obtained from the reconstruction model includes 3D pore distributions with color based on size or volume as shown in Figure 16.

3.5.3. Porosity.

Tables 2 and 3 show the effects of sulfate attack on the porosity of concrete. In the procedure of sulfate attack, the porosity of the concrete first decreased and then increased. This is consistent with the change in the average CT number. After 21 days, specimen porosity decreased by 11.6% and 6.3% for DW-1 and DW-2, respectively. For the reasons analyzed above, the porosity of the specimen decreased, which was attributed to the expansive products of the ettringite and gypsum as well as sulfate crystallization filling effect. At 42 days of sulfate attack, there was an increase in porosity because the swelling forces of the sulfate attack products and sulfate crystallization pressure acted on the pore walls. The resulting force of the two bodies exceeded the filling effect and drove the specimen porosity up to 2.06% and 3.41% for DW-1 and DW-2, respectively. After 63 days of sulfate attack, the pore connectivity was accelerated, and the volume of the pores increased eventually leading to microcracks being initiated and expanded. The specimen's internal porosity increased by 14.2% and 66%, and the specimen's overall structure became very loose. Tables 2 and 3 also indicate that the sulfate attack had a substantial impact on the number of internal micropores in the concrete. After 63 days, the total number of micropores increased by 15% and 31% for DW-1 and DW-2, respectively. The law of pore evolution is illustrated in Figure 17.

3.5.4. Pore Distribution Characteristics.

The pore-volume distributions of DW-1 and DW-2 were counted and are shown in Tables 4 and 5. Pores with a volume of $0.5–1$ mm^3 dominated the specimens. Pores with volumes in the range of $0.5–1$ mm^3 increased and then decreased throughout the experiment. The reason is due to ettringite, gypsum, and salt crystals filled the large pores and caused increase in small pores. With the continuous effect of swelling force and sulfate crystallization pressure, the small pores ($0.5–1$ mm^3)

TABLE 4: Pore distribution of DW-1 exposed to drying-wetting cycles with sulfate attack.

Pore volume (mm^3)	Sulfate attack period (day)			
	0 days	21 days	42 days	63 days
0–0.5	123	366	112	100
0.5–1.0	272	319	247	371
1.0–2.5	177	157	110	117
2.5–5.5	184	158	175	176
5.5–10	104	94	39	27

TABLE 5: Pore distribution of DW-2 exposed to drying-wetting cycles with sulfate attack.

Pore volume (mm^3)	Sulfate attack period (day)			
	0 days	21 days	42 days	63 days
0–0.5	266	103	64	81
0.5–1.0	239	233	137	237
1.0–2.5	137	173	176	183
2.5–5.5	162	166	173	186
5.5–10	140	155	171	140

began to connect and quickly aggregate into larger pores ($5.5–10$ mm^3) at 42 days of sulfate attack. After 63 days of sulfate attack, the pore volume with $0–5.5$ mm^3 increased and pore volume with $5.5–10$ mm^3 decreased. The reason for this may be as follows: (1) the microcracks expanded and cut through the larger pores significantly increasing the quantity of the small pores and (2) the small pores increased as expansion pressure caused by sulfate crystals created new pores.

3.5.5. Change in Porosity with Uniaxial Compressive Strength.

The relationship between porosity and uniaxial compressive strength of DW-1 and DW-2 specimens is plotted in Figure 18. As the sulfate attack progressed, the volume porosity decreased, and there was a negative correlation between the uniaxial compressive strength and porosity. The porosity of concrete has an important effect on concrete's mechanical properties and macrodamage characteristics. When the porosity was around 2%, the uniaxial
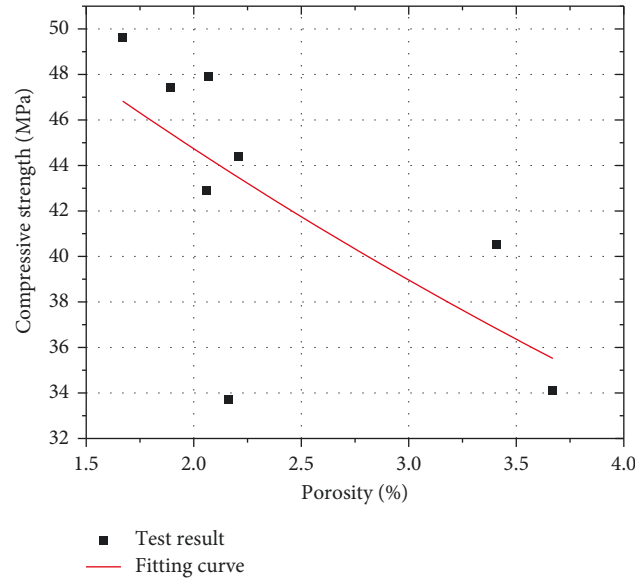
FIGURE 18: Relationship between porosity and uniaxial compressive strength.

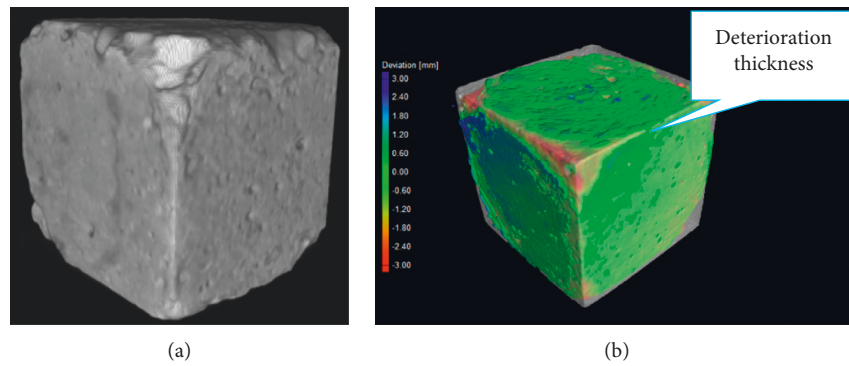(a)   (b)

FIGURE 19: The deterioration thickness of concrete specimen (63 days). (a) Deterioration surface and (b) deterioration thickness.

compressive strength changed rapidly indicating that the expansion of the pore degraded the mechanical properties. The uniaxial compressive strength reached the minimum when the porosity was 3.76%. Equation (3) was obtained by fitting the test data:

$$f_c = \left[e^{(4.07-0.138p)} \right], \qquad (3)$$

where p is the porosity and f_c is the uniaxial compressive strength.

3.6. Pore Regional Division Characteristics.

The sulfate mainly acted on the surface of the concrete, which due to specimens' inner pores were mostly closed and the infiltration pathways were not connected. As Figure 19(a) displays, the significant sanding and pitting occurred on the surface of the specimen. It indicated the specimen's thickness (green color) after 63 days of sulfate attack, the thickness and depth of deterioration region near the surface of the specimen increased, and small cracks and connected pores formed during the sulfate attack period

(Figure 19(b)). The solution more readily infiltrated the specimen over time to the point where it affected the internal pore regions of the specimen. So, we propose the pore regional division modeled in Figure 20(a): (1) Region 1 is one-fourth of the global region—a 25 mm × 25 mm cube central region; (2) Region 2 is one-half of the global region—a 50 mm × 50 mm cube area; and (3) Region 3 is the global region. Based on the pore regional division method, the 3D reconstruction of pores' structure in different divided regions is displayed in Figure 20(b).

3.6.1. Porosity of Regional Division.

Figure 21 and Table 6 display that the porosity in different regions of the specimens exposed to drying-wetting cycles during sulfate attack. Porosity first increased and then decreased in Region 3, but these changes were little complicated in Regions 1 and 2. In the early period of sulfate attack, sulfate ions entered the pores in the material and gradually infiltrated it. Region 3 experienced a significant decrease in porosity during the first 21 days of sulfate attack. This was mainly due to the formation of gypsum, ettringite, and other precipitation
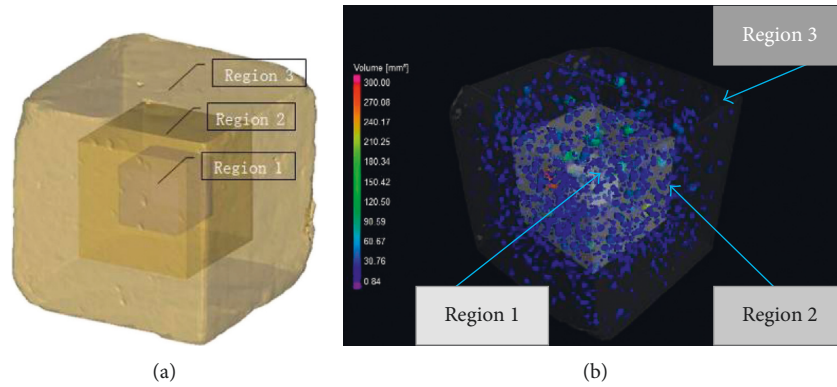
(a)

(b)

FIGURE 20: 3D view of pore's structure in different divided regions with color-coded pores according to size. (a) Pore divided region schemes and (b) 3D reconstruction of pore's structure in different divided regions (42 days of sulfate attack).
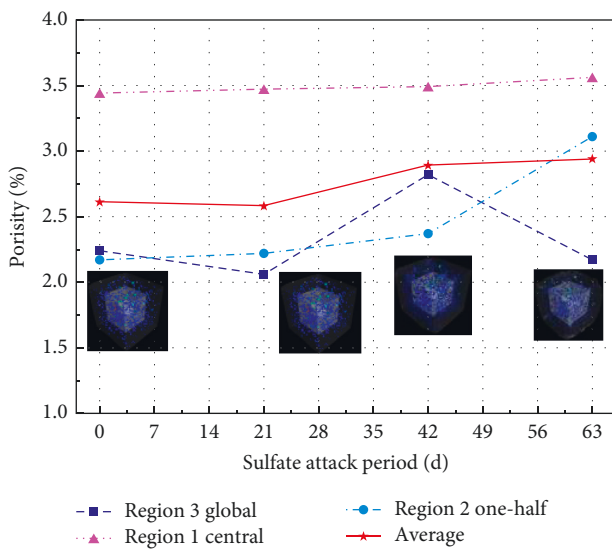

FIGURE 21: Porosity and pore volume in different divided regions in specimens exposed to drying-wetting cycles with sulfate attack.

TABLE 6: Porosity and pore volume in different divided regions in specimens exposed to drying-wetting cycles with sulfate attack.

ROI	Total porosity (%)			
	0 days	21 days	42 days	63 days
Region 3 global	2.24	2.06	2.82	2.17
Region 2 one-half	2.17	2.22	2.37	3.10
Region 1 central	3.43	3.46	3.48	3.55
Average	2.61	2.58	2.89	2.94

products as well as the salt crystal filling action. Regions 1 and 2 indicated slight increases in porosity, and the cause for this may be (1) pore water was converted to gas overflow through the drying-wetting cycles, which increased the size of the pores and thus their connectivity. (2) Regions 1 and 2 were not significantly affected by the sulfate solution as pore infiltration paths were not formed. After 42 days of sulfate attack, there was a significant increase in porosity in Region 3 due to the combined action of sulfate attack products'
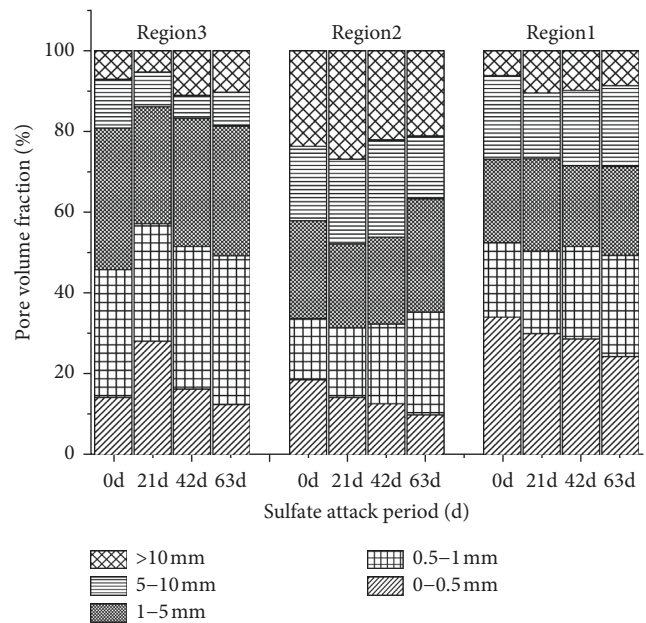

FIGURE 22: Pore volume of different regions with sulfate attack period in different divided regions.

swelling force and sulfate crystallization pressure. At this stage, cracks and pores in Region 3 allowed for solution infiltration leaving Region 2 susceptible to the sulfate as porosity continued to increase. After 63 days of sulfate attack, global porosity of Region 3 abruptly decreased due to local pitting and sanding. The porosity of Region 2 also increased at this point due to the constant expansion of the pores that were affected by solution infiltration. Region 1 central portions of the specimen were only affected by the drying-wetting cycle—their porosity continued to slightly increase throughout the experiment.

3.6.2. Pore Volume Distribution Characteristics of Regional Division. The pore-volume distributions of concrete are illustrated in Figure 22. The five characteristic ranges of pore volumes with corresponding distribution were observed: 0–0.5 mm^3, 0.5–1 mm^3, 1–5 mm^3, 5–10 mm^3, and >10 mm^3.

As shown in Figure 22, Region 3 of specimens was different in the pore distribution from Region 1 and Region 2.

In the Region 3 of specimens, the pores with volume 0.5–1 mm^3 were 36.7% of total pore volume, which was higher than the other pore-volume proportions. These ranges of pore volume first increased and then decreased during sulfate attack period. The reason is mainly due to the large pore space was filled, and thereby, the great number of small pores also emerged at the sulfate attack period. As the sulfate attack progressed, the small pores continuously emerged and developed, and the larger pores were formed. In Region 2 of specimens, the pores with volume more than 10 mm were mostly inside in this region. These pore volumes showed an increased and then decreased trend. As per the above analysis, when pore infiltration path was formed, the sulfate solution acted on the pore wall and made the pore volume increased. After 63 days of sulfate attack, the surface of specimens suffered macrodamage causing the large pore volume decrease. In Region 1 of specimens, the pores with volume 0-0.5 mm take up 34.2% higher than the other pore-volume proportions. These ranges of pore volume continued to decrease throughout the experiment. It indicates that this region is little significantly affected by the sulfate attack, and drying-wetting cycle was the main factor of the change in pore volume.

4. Conclusion

The behavior of concrete under sulfate attack and repeated drying-wetting cycles was investigated in this study. Our conclusions can be summarized as follows:

(1) Macroperformance was investigated via its apparent properties, mass loss, and compressive strength. Mass loss decreased initially due to the formation of expansive products by cement hydration. Mass loss increased in the middle stages of sulfate attack as hydration products such as C-S-H and calcium hydroxide gradually dissolved from the surface destroying the bonds between the aggregate and the mortar. The uniaxial compressive strength of the concrete specimen increased at the beginning of the drying-wetting cycles but then decreased over time.

(2) 3D pore structure of concrete specimens was reconstructed under the action of sulfate attack. The porosity and pore distributions changed over time in all specimens. After 21 days, the porosity decreased by 11.6% and 6.3% for DW-1 and DW-2 specimens, respectively. After 42 days, the porosity increased to 23.3% and 64.8% due to swelling force of the sulfate attack products and the sulfate crystallization pressure acting on the pore walls, respectively. After 63 days, the specimen's internal porosity increased by 4.8% and 7.6% for DW-1 and DW-2, respectively, and the specimen's structure became very loose. Pores with 0.5–1 mm^3 in volume dominated the specimens at this point. After 63 days, the pore volume decreased, and the quantity of micropores increased, indicating that the pressure caused by crystal expansion created new pores. Microcracks also expanded and cut through larger pores.

(3) The pore partition analysis showed significant differences in porosity and pore-volume distribution across different regions. Porosity decreased and then increased in the global region, but these changes were more complicated inside the one-half region and the central region. Region 3 of specimens is different in the pore distribution from Region 1 and Region 2. In Region 3 of specimens, the pores with volume 0.5–1 mm^3 were higher than the other pores with volume proportions. In Region 2 of specimens, the pores with volume more than 10 mm were mostly inside in this region. These pore volumes showed an increased and then decreased trend. In Region 1 of specimens, the pores with volume more than 0–0.5 mm take up 34.2% higher than the other pore-volume proportions. These pore volumes continued to decrease throughout the experiment.

Conflicts of Interest

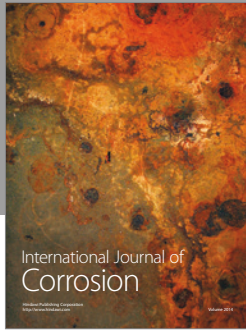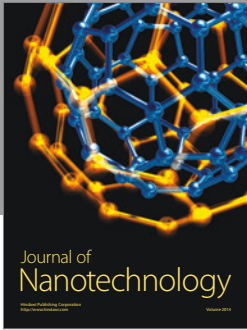The authors declare that they have no conflicts of interest.

Acknowledgments

References

[1] P. K. Mehta, P. Schiessl, and M. R. aupach, "Performance and durability of concrete systems," in *Proceedings of 9th International Congress of the Chemistry of Cement*, pp. 571–659, New Delhi, India, 1992.

[2] C. D. Laurence, "Sulphate attack on concrete," *Magazine of Concrete Research*, vol. 42, no. 153, pp. 249–264, 1990.

[3] B. Lothenbach, B. Bary, P. Le Bescop, T. Schmidt, and N. Leterrier, "Sulfate ingress in Portland cement," *Cement and Concrete Research*, vol. 40, no. 8, pp. 1211–1225, 2010.

[4] J. Prasad, D. K. Jain, and A. K. Ahuja, "Factors influencing the sulphate resistance of cement concrete and mortar," *Asian Journal of Civil Engineering*, vol. 7, no. 3, pp. 259–268, 2006.

[5] N. Thaulow and S. Sahu, "Mechanism of concrete deterioration due to salt crystallization," *Materials Characterization*, vol. 53, no. 2–4, pp. 123–127, 2004.

[6] A. R. Suleiman, A. M. Soliman, and M. L. Nehdi, "Effect of surface treatment on durability of concrete subjected to physical sulfate attack," *Construction and Building Materials*, vol. 73, pp. 674–681, 2014.

[7] H. Okochi, H. Kameda, and S. I. Hasegawa, "Deterioration of concrete structures by acid deposition—an assessment of the role of rainwater on deterioration by laboratory and field exposure experiments using mortar specimens," *Atmospheric Environment*, vol. 34, no. 18, pp. 2937–2945, 2000.

[8] R. Vedalakshmi, V. Saraswathy, and A. K. Yong, "Performance evaluation of blended cement concretes under MgSO$_4$

attack," *Magazine of Concrete Research*, vol. 63, no. 9, pp. 669–681, 2011.

[9] T. H. Wee, A. K. Suyavanshi, S. F. Wong, and A. K. M. A. Rahman, "Sulfate resistance of concrete containing mineral admixtures," *Materials Journal*, vol. 97, no. 5, pp. 536–549, 2000.

[10] S. U. Al-Dulaijan, M. Maslehuddin, M. M. Al-Zahrani, A. M. Sharif, M. Shameem, and M. Ibrahim, "Sulfate resistance of plain and blended cements exposed to varying concentrations of sodium sulfate," *Cement and Concrete Composites*, vol. 25, no. 4-5, pp. 429–437, 2003.

[11] Z. Q. Jin, W. Sun, Y. S. Zhang, J. Y. Jiang, and J. Z. Lai, "Interaction between sulfate and chloride solution attack of concretes with and without fly ash," *Cement and Concrete Research*, vol. 37, no. 8, pp. 1223–1232, 2007.

[12] D. M. Yu, B. M. Guan, R. He, R. Xiong, and Z. Liu, "Sulfate attack of Portland cement concrete under dynamic flexural loading: a coupling function," *Construction and Building Materials*, vol. 115, pp. 478–485, 2016.

[13] L. Jiang and D. T Niu, "Study of deterioration of concrete subjected to different types of sulfate solutions under drying-wetting cycles," *Construction and Building Materials*, vol. 117, pp. 88–98, 2016.

[14] D. T. Niu, Y. D. Wang, R. Ma, J. B. Wang, and S. H. Xu, "Experiment study on the failure mechanism of dry-mix shotcrete under the combined actions of sulfate attack and drying-wetting cycles," *Construction and Building Materials*, vol. 81, pp. 74–80, 2015.

[15] J. Yuan, Y. Liu, Z. C. Tan, and B. K. Zhang, "Investigating the failure process of concrete under the coupled actions between sulfate attack and drying–wetting cycles by using X-ray CT," *Construction and Building Materials*, vol. 108, pp. 129–138, 2016.

[16] M. Santhanam, D. M. Cohen, and J. Olek, "Mechanism of sulfate attack: a fresh look part 2: proposed mechanisms," *Cement and Concrete Research*, vol. 33, no. 3, pp. 341–346, 2003.

[17] C. X. Qian, Y. F. Nie, and T. J. Cao, "Sulphate attack-induced damage and micro-mechanical properties of concrete characterized by nano-indentation coupled with X-ray computed tomography," *Structural Concrete*, vol. 17, no. 1, pp. 96–104, 2016.

[18] N. N. Naik, A. C. Jupe, S. R. Stock, A. P. Wilkinson, P. L. Lee, and K. E. Kurtis, "Sulfate attack monitored by micro CT and EDXRD: influence of cement type, water-to-cement ratio, and aggregate," *Cement and Concrete Research*, vol. 36, no. 1, pp. 144–159, 2006.

[19] R. El-Hachem, E. Rozière, F. Grondin, and A. Loukili, "Multi-criteria analysis of the mechanism of degradation of Portland cement based mortars exposed to external sulphate attack," *Cement and Concrete Research*, vol. 42, no. 10, pp. 1327–1335, 2012.

[20] National Standards of People's Republic of China (NSPRC), *Standard for Test Method of Long-Term Performance and Durability of Ordinary Concrete, GB/T 50082–2009*, China Architecture and Building Press (CABP), Beijing, China, 2009, in Chinese.

[21] National Standards of People's Republic of China (NSPRC), *Standard for Test Method of Mechanical Properties on Ordinary Concrete, GB/T 50081–2002*, China Architecture and Building Press (CABP), Beijing, China, 2002, in Chinese.

[22] W. Tian and N. Han, "Evaluation of damage in concrete suffered freeze-thaw cycles by CT technique," *Journal of Advanced Concrete Technology*, vol. 42, no. 11, pp. 679–690, 2016.